Inorg. Chem. **2009**, *48*, 28−35

Identification of the Reactive cis,mer Isomer of $[Ir(CO)_2I_3Me]^-$: Relation to the Mechanism of Iridium-Catalyzed Methanol Carbonylation

Anthony Haynes,* Anthony J. H. M. Meijer,* James R. Lyons, and Harry Adams

Department of Chemistry, University of Sheffield, Sheffield, S3 7HF, United Kingdom

Received September 18, 2008

Thermal dissociation of CO from *cis,fac*-$[Ir(CO)_2I_3Me]^-$ (**1a**) gives the iodide-bridged dimer $[\{Ir(CO)I_2(\mu\text{-}I)Me\}_2]^{2-}$, which was characterized crystallographically as its Ph_4As^+ salt. This dimer reacts with CO at ambient temperature to give the acetyl complex *trans,mer*-$[Ir(CO)_2I_3(COMe)]^-$. An intermediate in this reaction is the previously unobserved *cis,mer*-$[Ir(CO)_2I_3Me]^-$ (**1b**), which was characterized by IR and NMR spectroscopy. Carbonylation of **1b** is much faster ($t_{1/2} \sim 1$ min at 25 °C) than for the cis,fac isomer **1a** and also faster than the neutral tricarbonyl $[Ir(CO)_3I_2Me]$. The observations show that the *relative positioning* of carbonyl ligands influences reactivity more than than their *number*, and that CO insertion is particularly accelerated when a CO ligand is placed trans to the migrating methyl group. DFT calculations indicate that the Ir−CO bond trans to methyl contracts significantly as **1b** approaches the transition state for methyl migration, facilitating stronger π-backbonding from Ir to the spectator CO ligand, which stabilizes the transition state. The results confirm the recently proposed CO-loss mechanism for the photochemical carbonylation of **1a** and suggest that the cis,mer isomer may play a minor role in the catalytic cycle for methanol carbonylation.

Introduction

The BP Chemicals Cativa process[1] for the carbonylation of methanol now operates commercially in several plants, using a promoted iridium/iodide catalyst. The catalytic cycle has been studied in detail and involves rate-determining carbonylation of an anionic Ir(III) methyl species, *cis,fac*-$[Ir(CO)_2I_3Me]^-$, **1a**.[2−5] This reaction is promoted by iodide acceptors but inhibited by iodide salts, and the dominant mechanism is thought to proceed via substitution of the iodide trans to methyl by CO (Scheme 1). Consistent with this, the neutral tricarbonyl *fac,cis*-$[Ir(CO)_3I_2Me]$ was characterized spectroscopically and shown to undergo migratory CO insertion at a rate substantially faster than that for **1a**.[4,5]

Scheme 1. Iodide-Loss Mechanism for Carbonylation of **1a**

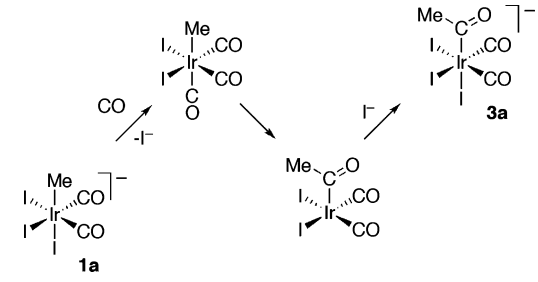

In a recent study, Volpe et al. found that stoichiometric carbonylation of **1a** to *trans,mer*-$[Ir(CO)_2I_3(COMe)]^-$ (**3b**) could be promoted photochemically.[6] A mechanism was proposed (Scheme 2) in which the photodissociation of CO gives the monocarbonyl $[Ir(CO)I_3Me]^-$ (**2a**) followed by rearrangement to place the vacant site trans to methyl (**2b**). Coordination of CO to **2b** was proposed to give *cis,mer*-$[Ir(CO)_2I_3Me]^-$ (**1b**). On the basis of predictions made in a computational (DFT) study,[7] it was suggested that **1b** undergoes migratory CO insertion much more easily than the "normal" isomer **1a**. Time-resolved infrared kinetic data

* Authors to whom correspondence should be addressed. E-mail: a.haynes@sheffield.ac.uk (A.H.), a.meijer@sheffield.ac.uk (A.J.H.M.M.).

(1) Sunley, G. J.; Watson, D. J. *Catal. Today* **2000**, *58*, 293.
(2) Forster, D. *J. Chem. Soc., Dalton Trans.* **1979**, 1639.
(3) Pearson, J. M.; Haynes, A.; Morris, G. E.; Sunley, G. J.; Maitlis, P. M. *J. Chem. Soc., Chem. Commun.* **1995**, 1045.
(4) Ghaffar, T.; Adams, H.; Maitlis, P. M.; Sunley, G. J.; Baker, M. J.; Haynes, A. *Chem. Commun.* **1998**, 1023.
(5) Haynes, A.; Maitlis, P. M.; Morris, G. E.; Sunley, G. J.; Adams, H.; Badger, P. W.; Bowers, C. M.; Cook, D. B.; Elliott, P. I. P.; Ghaffar, T.; Green, H.; Griffin, T. R.; Payne, M.; Pearson, J. M.; Taylor, M. J.; Vickers, P. W.; Watt, R. J. *J. Am. Chem. Soc.* **2004**, *126*, 2847.
(6) Volpe, M.; Wu, G.; Iretskii, A.; Ford, P. C. *Inorg. Chem.* **2006**, *45*, 1861.
(7) Kinnunen, T.; Laasonen, K. *THEOCHEM* **2001**, *542*, 273.

10.1021/ic8017858 CCC: $40.75
Published on Web 12/05/2008

Scheme 2. Mechanism Proposed by Volpe et al. for Photochemical Carbonylation of **1a**[6]

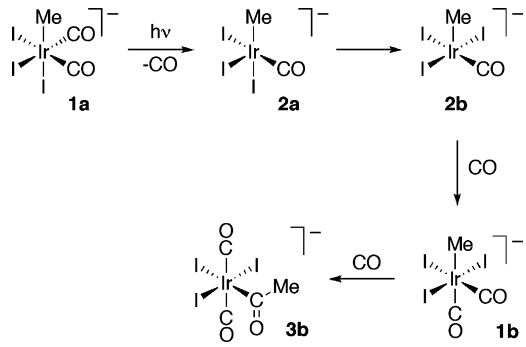

Scheme 3. Thermal Decarbonylation of **1a** to Give **2d**

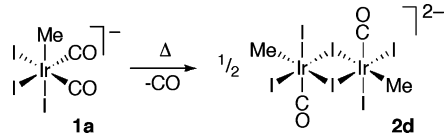

from flash photolysis experiments reported by Volpe et al. were consistent with the proposed CO-loss pathway, but although some transient IR absorptions were observed, no definitive assignments to the key intermediates, **2a/b** and **1b**, were made.

In this paper, we report a study of the thermal CO dissociation chemistry of **1a**. Our results demonstrate conclusively that the isomerization **1a** → **1b** can proceed via a CO-loss pathway, and the results confirm that migratory CO insertion occurs under much milder conditions for **1b** than for **1a**. The new isomer, **1b**, is characterized by IR and NMR spectroscopy aided by ^{13}C isotopic labeling, and its reactivity is probed by a stopped flow-kinetic study. We also report a detailed DFT study of the reaction coordinates for methyl migration and CO dissociation in this system.

Results and Discussion

Decarbonylation of 1a. Initial attempts to remove a carbonyl ligand from **1a** employed amine oxides that are known to effect decarbonylation by oxidizing a CO ligand to CO_2. When trimethyl amine oxide or N-methyl morpholine N-oxide were used, spectroscopic evidence did suggest the formation of monocarbonyl species, but no pure product could be isolated. In one case, crystals were obtained which X-ray crystallography showed to contain a di-iridium complex, [Me(CO)(I)Ir(μ-I)$_2$(μ-OH)Ir(CO)(I)Me]$^-$ (see the Supporting Information). Each of the Ir centers in this complex has a single carbonyl ligand, demonstrating that a loss of CO has occurred, and the bridging hydroxy group presumably arises from the presence of trace water. Mass spectroscopy indicated the formation of other di-iridium complexes such as [Me(CO)(I)Ir(μ-I)$_3$Ir(CO)(I)Me]$^-$, as well as the [Ir(CO)I$_3$Me]$^-$ fragment.

Since the amine oxide reactions did not afford a clean isolable product, we investigated whether the desired decarbonylation could be achieved in a simple thermal process. Complex **1a** is relatively robust, although reductive elimination of methyl iodide can occur at elevated temperatures.[8] In order to prevent this potential side reaction, our attempts to induce thermal CO loss were carried out in the presence of excess methyl iodide. Prolonged reflux of a chlorobenzene/MeI solution of **1a**[AsPh$_4$] was found to lead to precipitation of an orange product for which elemental analysis is consistent with an empirical formula of [Ir(CO)I$_3$Me]AsPh$_4$. The product displays a single ν(CO) absorption at 2029 cm^{-1} (CH_2Cl_2), consistent with a monocarbonyl complex.[9] This band is shifted to low frequency compared with those of the reactant (2098, 2045 cm^{-1}), as expected upon the loss of a π-acceptor CO ligand. The negative ion ESI mass spectrum has a strong peak at *m*/*z* 617, corresponding to [Ir(CO)I$_3$Me]$^-$.

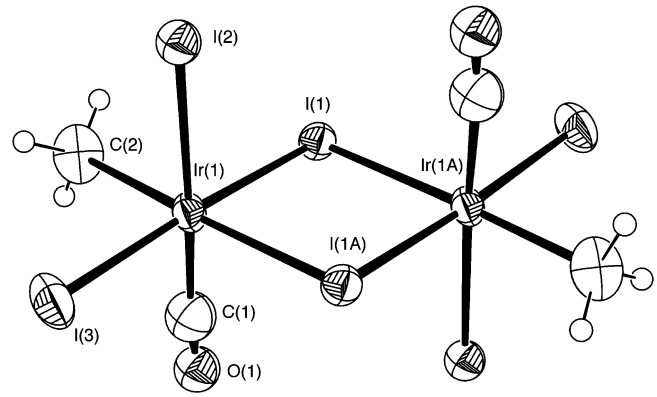

Figure 1. ORTEP plot for complex **2d**. Thermal ellipsoids are shown at the 50% probability level. Ph$_4$As$^+$ counterions and disordered iodides are omitted for clarity.

Table 1. Selected Bond Lengths (Å) and Bond Angles (deg) for **2d**

Ir(1)−C(1)	1.887(13)	C(2)−Ir(1)−I(3)	87.8(3)
Ir(1)−C(2)	2.200(10)	C(1)−Ir(1)−I(1)	89.2(4)
Ir(1)−I(1)	2.6819(10)	C(1)−Ir(1)−I(3)	88.2(4)
Ir(1)−I(2)	2.7189(11)	I(1)−Ir(1)−I(2)	90.08(2)
Ir(1)−I(3)	2.6592(10)	I(3)−Ir(1)−I(2)	92.70(3)
Ir(1)-I(1A)	2.8082(10)	I(3)−Ir(1)−I(1)	176.82(2)
O(1)−C(1)	1.023(16)	C(1)−Ir(1)−I(2)	175.6(4)
C(1)−Ir(1)−C(2)	90.7(4)	C(2)−Ir(1)−I(1A)	176.6(2)
C(2)−Ir(1)−I(1)	94.0(3)	Ir(1)−I(1)−Ir(1A)	93.15(2)
C(2)−Ir(1)−I(2)	85.1(2)	O(1)−C(1)−Ir(1)	175.1(11)

A crystal suitable for an X-ray diffraction study was obtained by the slow diffusion of Et$_2$O into a CH_2Cl_2 solution of the compound, and the resulting structure revealed a dinuclear complex, [{Ir(CO)I$_2$(μ-I)Me}$_2$]$^{2-}$ (**2d**, Scheme 3). This structure adopts the same space group ($P\bar{1}$) and has very similar unit cell dimensions as those reported by Volpe et al. for the related acetyl dimer [{Ir(CO)I$_2$(μ-I)(COMe)}$_2$]·2AsPh4.[6] The structure of the anion is illustrated in Figure 1, and geometric data are given in Table 1. The centrosymmetric dimer can be regarded as two square-pyramidal [Ir(CO)I$_3$Me]$^-$ units linked through bridging iodide ligands. Some disorder is present, involving I(2) and the carbonyl ligand trans to it. The geometry around each Ir center is approximately octahedral, and none of the bond angles between cis ligands deviate from the ideal by more than 5°. The Ir−(μ-I) distance trans to methyl is significantly

(8) Vickers, P. W.; Pearson, J. M.; Ghaffar, T.; Adams, H.; Haynes, A. *J. Phys. Org. Chem.* **2004**, *17*, 1007.

(9) This ν(CO) band is close to a transient IR absorption at 2032 cm^{-1} observed after the flash photolysis of **1a** by Volpe et al. (ref 6).

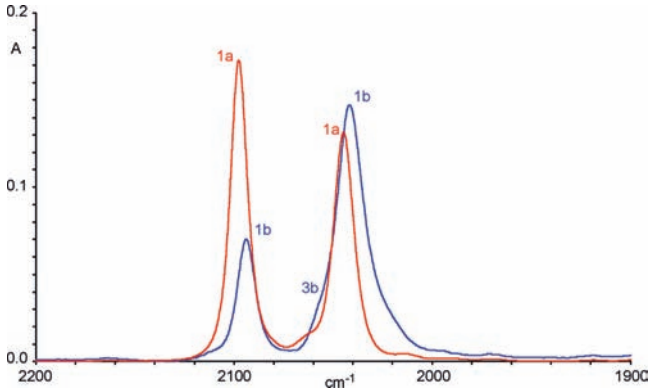

Figure 2. IR spectra illustrating small shifts to low frequency and different relative intensities of ν(CO) bands of **1b** (blue) compared with those of **1a** (red). The weak shoulder in the spectrum of **1b** is due to the presence of some **3b**.

longer than the other Ir−I distances, reflecting the strong trans influence of methyl, as found in the structures of related complexes.[5,6,10]

Reactivity of 2d with Carbon Monoxide. The dimer **2d** can be regarded as a "trapped" form of the monocarbonyl intermediate **2b** proposed by Volpe et al.[6] It was therefore of interest to study the reaction of **2d** with CO: would this simply regenerate **1a** or lead to the proposed more reactive dicarbonyl isomer **1b** and subsequent methyl migration? The bubbling of CO through a CH_2Cl_2 solution of **2d**$[AsPh_4]_2$ for 1−2 min at ambient temperature resulted in the disappearance of the IR band of **2d** at 2029 cm^{-1} and the formation of ν(CO) absorptions at 2064 and 1653 cm^{-1} corresponding to *trans*,*mer*-$[Ir(CO)_2I_3(COMe)]^-$ (**3b**). Formation of the acetyl complex **3b** was confirmed by ^{1}H NMR spectroscopy (δ ^{1}H 2.76). An X-ray crystal structure of **3b**$[AsPh_4]$ was also obtained (see the Supporting Information), in which the iridium anion displays a geometry very similar to that in two other recent crystallographic determinations of salts of this complex.[6,11,12] The facile formation of **3b** demonstrates that migratory CO insertion occurs rapidly under very mild conditions using **2d** as the iridium precursor.

Evidence for a reactive dicarbonyl intermediate in the carbonylation of **2d** was obtained by using IR spectroscopy to monitor the initial stages of the reaction. After CO was bubbled for 15 s through a CH_2Cl_2 solution of **2d**$[AsPh_4]_2$, two new absorptions were observed at 2094 and 2041 cm^{-1}. This pair of bands is consistent with a cis dicarbonyl species, with each absorption shifted by 3−4 cm^{-1} to low frequency relative to those of the cis,fac isomer **1a**, as illustrated in Figure 2. Vibrational frequencies calculated using DFT by Kinnunen and Laasonnen[7] and ourselves (see the Supporting Information) predict similar small differences in ν(CO) values between **1a** and **1b**. The relative intensities of the symmetric and antisymmetric ν(CO) modes predicted by DFT also

Scheme 4. Reaction of **2d** with CO

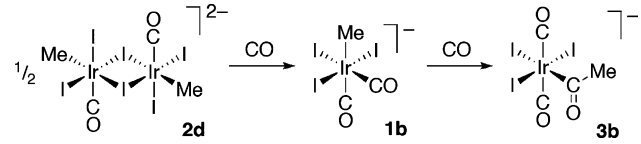

Scheme 5. Isotopic Labeling Experiments

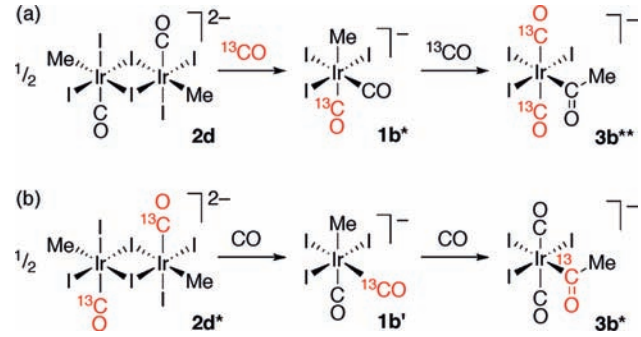

match qualitatively with experimental results. The different intensity pattern for **1b** presumably results from the different local oscillating dipoles associated with the inequivalent CO ligands. On continued reaction with CO, the bands assigned to **1b** decayed with the growth of absorptions due to the acetyl product **3b**. This clearly demonstrates that the absorptions at 2094 and 2041 cm^{-1} are not due to the "normal" dicarbonyl isomer **1a**, since that complex is unreactive toward CO under these mild conditions. The IR spectroscopic data for the reaction of **2d** with CO are therefore consistent with the reaction sequence shown in Scheme 4.

Further IR spectroscopic evidence to support the intermediacy of **1b** in this reaction was obtained from ^{13}C isotopic labeling experiments. The treatment of nonlabeled **2d**$[AsPh_4]_2$ with ^{13}CO in CH_2Cl_2 gave an intermediate with ν(CO) bands at 2071 and 2019 cm^{-1}. Conversely, 80% ^{13}CO-labeled **2d***$[AsPh_4]_2$ reacted with unlabeled CO to give a major species with ν(CO) bands at 2086 and 2002 cm^{-1}. These pairs of bands are assigned to the singly labeled isotopomers **1b*** and **1b′**, respectively, each resulting from the incoming CO ligand binding trans to methyl (Scheme 5). The different ν(CO) frequencies observed for **1b*** and **1b′** clearly indicate inequivalent CO ligands, and the observed frequencies can be modeled satisfactorily by a CO-factored force field,[13] in which the stretching force constant for the CO ligand trans to methyl (CO_{trans}) is ca. 40 N m^{-1} larger than that for the CO cis to methyl (CO_{cis}). Less π back-donation is therefore experienced by CO_{trans}, as found previously for *fac*,*cis*-$[Ir(CO)_3I_2Me]$.[4]

The acetyl products ultimately formed in the ^{13}C-labeling experiments are also consistent with the proposed mecha-

(10) Gautron, S.; Giordano, R.; Le Berre, C.; Jaud, J.; Daran, J.-C.; Serp, P.; Kalck, P. *Inorg. Chem.* **2003**, *42*, 5523.

(11) Gautron, S.; Lassauque, N.; Le Berre, C.; Azam, L.; Giordano, R.; Serp, P.; Laurenczy, G.; Daran, J.-C.; Duhayon, C.; Thiébaut, D.; Kalck, P. *Organometallics* **2006**, *25*, 5894.

(12) In the structure obtained in this study, [**3b**]$AsPh_4$ crystallizes in a different space group ($P2_1/c$) than that in the structure reported by Volpe et al. ($P\bar{1}$, ref 6).

(13) The observed ν(CO) frequencies for isotopomers of **1b** were modeled by a CO factored force field (based on the analysis by Braterman in *Metal Carbonyl Spectra*; Academic Press: London, 1975) to give the following C−O stretching (k) and interaction (i) force constants for **1b**: k_c = 1707.1 N m^{-1} (CO cis to Me), k_t = 1746.7 N m^{-1} (CO trans to Me), and i = 38.6 N m^{-1} (see the Supporting Information for calculated ν(CO) frequencies). A similar analysis for the cis,fac isomer **1a** gives values of k_c = 1734 N m^{-1} and i = 43.2 N m^{-1}. The shift to low frequency of the ν(CO) bands of **1b** relative to **1a** is therefore due to a lower *average* value of k for the inequivalent CO ligands in **1b** (despite the higher value of k_t).

nism. The reaction of **2d** with ^{13}CO ultimately gives **3b**** with a terminal $\nu(^{13}CO)$ band at 2019 cm^{-1} and an acetyl $\nu(^{12}CO)$ band at 1656 cm^{-1}. The absence of $^2J_{CH}$ coupling for a singlet at δ 2.76 in the ^1H NMR spectrum confirms that the ^{13}CO label is not incorporated into the acetyl ligand. Conversely, **3b***, formed from the reaction of 80% ^{13}CO-labeled **2d*** with unlabeled CO, has the ^{13}CO label incorporated into its acetyl ligand, as judged by IR and ^1H NMR intensity patterns.[14] These results confirm that the acetyl ligand of **3b** arises from the migration of methyl to the CO ligand originally present in **2d** and not one of the incoming CO molecules. This also establishes the inequivalence of the two CO ligands in **1b**, with the incoming CO ligand coordinating trans to methyl.

Complex **1b** was also characterized using ^{13}C NMR spectroscopy. After treatment of a CD_2Cl_2 solution of $[\{Ir(^{13}CO)I_2(\mu\text{-}I)(^{13}CH_3)\}_2][AsPh_4]_2$ with ^{13}CO (brief bubbling followed by purging with N_2), the $^{13}C\{^1H\}$ NMR spectrum displayed a doublet of doublets for the methyl carbon at δ −18.96 ($^2J_{CC}$ = 33 and 3 Hz) due to coupling with two inequivalent carbonyl ligands. The widely different $^2J_{CC}$ values are consistent with coupling to trans and cis CO ligands, for which doublet of doublet signals were also observed (δ 160.55 ($^2J_{CC}$ = 33 and 1.5 Hz) for CO_{trans} and δ 156.20 ($^2J_{CC}$ = 3 and 1.5 Hz) for CO_{cis}). The ^1H NMR spectrum of ^{13}C-labeled **1b** showed a doublet for the methyl ligand at δ 2.46 with a $^1J_{CH}$ of 137 Hz.

Complex **1b** was shown to be relatively stable in the absence of excess CO. Solid samples containing **1b** as the major Ir complex could be obtained after brief bubbling of CO through a CH_2Cl_2 solution of **2d**$[AsPh_4]_2$, followed by purging with N_2 and evaporation to dryness. The negative ion ES mass spectrum showed a weak molecular ion peak at *m*/*z* 645 for **1b** along with a stronger peak at *m*/*z* 617 corresponding to the loss of a CO ligand. However, attempts to isolate **1b**$[AsPh_4]$ as a pure solid or to obtain X-ray-quality crystals were unsuccessful.

Kinetics of the Migratory Insertion Reaction. Kinetic measurements on the reaction of **2d** with CO in CH_2Cl_2 were performed using stopped-flow infrared spectroscopy. Rapid decay of the ν(CO) band at 2029 cm^{-1} indicates that the dimer **2d** is cleaved by CO within a few seconds ($t_{1/2}$ ca. 4 s at 25 °C). This is accompanied by the growth of bands due to **1b** at 2094 and 2041 cm^{-1}, which then decay over a slower time scale ($t_{1/2}$ ca. 60 s at 25 °C) to give **3b**.[15] First-order rate constants for the carbonylation of **1b** were obtained from exponential fits to the absorbance versus time data for the ν(CO) band of **1b** at 2041 and are given in Table 2. Activation parameters were estimated from an Eyring plot

Table 2. Kinetic Data for the Reaction of **1b** with CO in CH_2Cl_2

temperature/°C	$10^3\ k_{obs}/s^{-1}$
14.8	5.11
18.1	6.36
21.0	7.74
23.1	10.0
25.3	11.9
27.3	17.3

of the variable-temperature data as $\Delta H^{\ddagger} = 62 \pm 7$ kJ mol^{-1} and $\Delta S^{\ddagger} = -73 \pm 23$ J $K^{-1}mol^{-1}$.[16]

Comparison with activation parameters reported for carbonylation of the cis,fac isomer **1a** ($\Delta H^{\ddagger} = 152 \pm 6$ kJ mol^{-1} and $\Delta S^{\ddagger} = 82 \pm 17$ J K^{-1} mol^{-1} in chlorobenzene)[5] illustrate the much higher reactivity of **1b** ($\Delta G^{\ddagger}_{298}$ ca. 84 vs 128 kJ mol^{-1}). The ease of carbonylation of **1b** even exceeds that of the neutral tricabonyl, *fac*,*cis*-$[Ir(CO)_3I_2Me]$, the key intermediate in which methyl migration is thought to occur during catalytic methanol carbonylation. Previously, we have ascribed the low activation barrier for the tricarbonyl (relative to **1a**) to the increased competition for π-backbonding brought about by coordination of a third CO ligand.[4,5] The present data suggest that the *relative positioning* of carbonyl ligands is more significant than their *number*, and that CO insertion is particularly accelerated when a CO ligand is placed trans to the migrating methyl group. In an early computational study[17] (using extended Hückel theory), Berke and Hoffmann found that coordination of a π-acceptor ligand in the migration plane would lower the activation energy for methyl migration on a d^6 metal center; this has been verified experimentally for $[Ir(CO)(PPh_3)_2(L)ClMe]$ (L = CO, isonitrile),[18] $[Ir(CO)_2(L)I_2Me]$ (L = phosphite),[19] and isomers of $[M(CO)_2(PMe_3)_2)IMe]$ (M = Fe,[20] Ru[21]). Computational results on the present system, which throw more light on the factors influencing the relative reactivity of isomers, are discussed in the following section.

DFT Calculations. DFT calculations by Kinnunen and Laasonen[7] (and later by Volpe et al.[6]) correctly predicted a much lower barrier for methyl migration in **1b** than in **1a** ($\Delta G^{\ddagger}_{298}$ ca. 69 and 120 kJ mol^{-1}, respectively). Their predicted barrier (86 kJ mol^{-1}) for *fac*,*cis*-$[Ir(CO)_3I_2Me]$ falls between those for **1a** and **1b** and so follows the trend established by experimentation. Kinnunen and Laasonen attributed the lower methyl migration barrier in **1b** to a trans effect of the CO ligand, but the origin of this trans effect was not discussed further. Ziegler and co-workers also reported DFT calculations on the $[Ir(CO)_2I_3Me]^-$ and $[Ir(CO)_3I_2Me]$ systems but did not consider methyl migration

(14) Spectroscopic data for **3b***: IR: $\nu(^{13}CO)$ 1619 cm^{-1} (major), $\nu(^{12}CO)$ 1653 cm^{-1} (minor) for the acetyl ligand; $\nu(^{12}CO)$ 2063 cm^{-1} for the terminal CO ligands. ^1H NMR: δ 2.76; $^2J_{CH}$ 5.2 Hz, strong doublet with intervening weak singlet.

(15) Weak IR bands at 2106 and 2060 cm^{-1} were also detected during the stopped-flow experiments, indicative of an intermediate, which we tentatively assign as a mono-iodide bridged complex, $[Me(CO)_2I_2Ir(\mu\text{-}I)Ir(CO)I_3Me]^{2-}$. This would result from the reaction of **2d** with 1 equiv of CO before complete cleavage of the dimer to give **1b**.

(16) Notably, the activation parameters reported here for **1b** are very similar to those for methyl migration in *cis*,*fac*-$[Rh(CO)_2I_3Me)]^-$ ($\Delta H^{\ddagger} = 63 \pm 2$ kJ mol^{-1} and $\Delta S^{\ddagger} = -59 \pm 9$ J K^{-1} mol^{-1}): (a) Haynes, A.; Mann, B. E.; Morris, G. E.; Maitlis, P. M. *J. Am. Chem. Soc.* **1993**, *115*, 4093.

(17) Berke, H.; Hoffmann, R. *J. Am. Chem. Soc.* **1978**, *100*, 7224.
(18) Kubota, M.; McClesky, T. M.; Hayashi, R. K.; Webb, C. G. *J. Am. Chem. Soc.* **1987**, *109*, 7569.
(19) Haynes, A.; Pearson, J. M.; Vickers, P. W.; Charmant, J. P. H.; Maitlis, P. M. *Inorg. Chim. Acta* **1998**, *270*, 382.
(20) Bellachioma, G.; Cardaci, G.; Jablonski, C.; Macchioni, A.; Reichenbach, G. *Inorg. Chem.* **1993**, *32*, 2404.
(21) Bellachioma, G.; Cardaci, G.; Macchioni, A.; Reichenbach, G. *J. Organomet. Chem.* **1997**, *540*, 7.

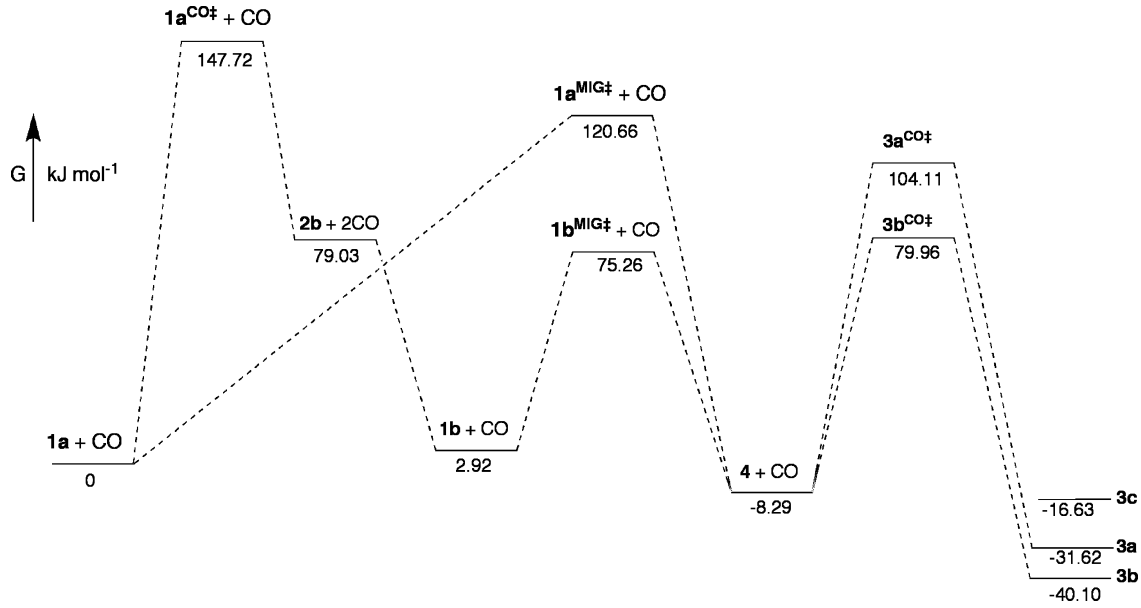

Figure 3. Free energy profile (B3LYP) calculated for carbonylation of **1a**.

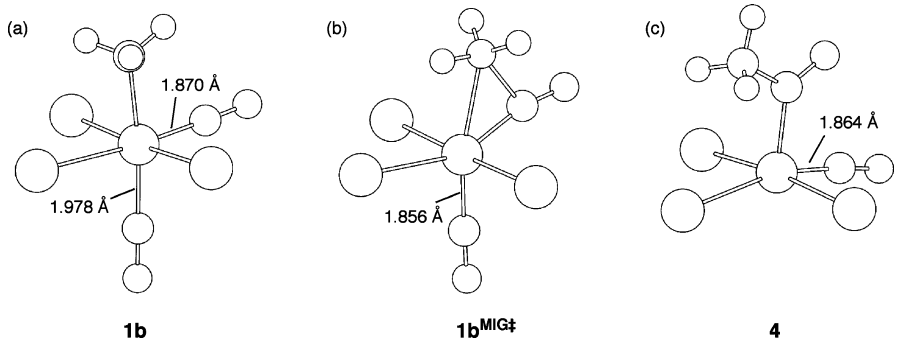

Figure 4. Optimized structures and Ir−CO distances for stationary points on the reaction coordinate for methyl migration in *cis*,*mer*-$[Ir(CO)_2I_3Me]^-$.

in the cis,mer isomer of $[Ir(CO)_2I_3Me]^-$.[22] We have therefore carried out DFT calculations independently to probe this system in more detail.

Reactant, product, and transition state geometries were optimized using the B3LYP functional (with counterpoise correction, see the Experimental Section) and are in close agreement with those reported in previous studies. Single-point CCSD(T) calculations were also performed on the B3LYP optimized geometries (see the Supporting Information). Relative free energies of the iridium species are shown in Figure 3. Complex **1b** is marginally higher in energy than **1a** in the B3LYP calculations, but this ordering is reversed in the single-point CCSD(T) results.[23] The structures of the two isomers do not indicate any significant weakening of the Ir−Me bond in the ground state of **1b** compared with **1a**. Indeed, the Ir−Me distance in **1b** is slightly *shorter*. A notable feature of the optimized geometry of **1b** (Figure 4a) is that the $Ir-CO_{trans}$ bond distance (1.978 Å) is significantly longer than $Ir-CO_{cis}$ (1.870 Å). This difference arises from the strong trans influence of the methyl ligand (relative to iodide) and has the consequence that π-backdonation from Ir to CO_{trans} will be weaker than to CO_{cis}, consistent with the experimental IR data (see above).

In agreement with previous reports, the transition state for methyl migration in the cis,mer isomer ($\mathbf{1b}^{MIG‡}$) is substantially lower in energy than that for the cis,fac isomer ($\mathbf{1a}^{MIG‡}$). Inspection of the geometry of $\mathbf{1b}^{MIG‡}$ (Figure 4b) reveals that the $Ir-CO_{trans}$ bond distance (1.856 Å) is ca. 6% shorter than in the ground-state **1b**. Intrinsic reaction coordinate (IRC) calculations show a smooth contraction of the $Ir-CO_{trans}$ bond upon progression from **1b** to the transition state, which can be can be attributed to a diminution of the trans influence of the migrating methyl ligand. The closer proximity to the metal center will enable CO_{trans} to act as a more effective π acceptor in the transition state, which will help to compensate for the decreasing π-acceptor ability of CO_{cis} as it forms the new acetyl ligand.[24] Although analysis of specific orbital contributions can be problematic in DFT, inspection of the energies of orbitals with significant Ir (d_π) → CO ($\pi*$) interactions indicates a greater retention of π-backbonding in the transition state $\mathbf{1b}^{MIG‡}$ than in $\mathbf{1a}^{MIG‡}$. Thus, a π-acceptor ligand trans to the migrating methyl ligand is uniquely placed to stabilize the transition state,

(22) Cheong, M.; Schmid, R.; Ziegler, T. *Organometallics* **2000**, *19*, 1973.
(23) The trans,mer isomer of $[Ir(CO)_2I_3Me]^-$ is calculated to be more stable than **1a** by 6.3 kJ mol^{-1} (B3LYP) and 7.2 kJ mol^{-1} (CCSD(T)).
(24) We note that Ziegler and co-workers calculated that the activation barrier for methyl migration in $[Ir(CO)_3I_2Me]$ is lower for isomers that have CO trans to methyl (ref 22).

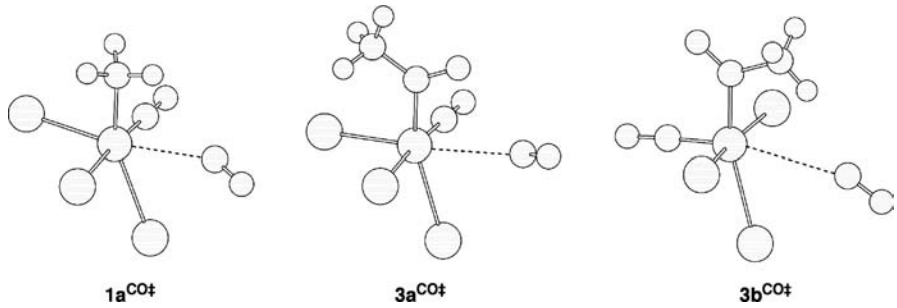

Figure 5. Optimized transition state structures for CO dissociation from Ir complexes **1a**, **3a**, and **3b**.

resulting in a considerably lower activation energy for methyl migration in **1b** than in **1a**.[25] For comparison, the calculations show that, during methyl migration in **1a**, the Ir−CO bond distance to the spectator carbonyl ligand is almost identical in the ground and transition states (1.882 vs 1.879 Å). In this case, the Ir−I bond trans to methyl contracts by ca. 6%, but since iodide is not a π-acceptor ligand, this does not stabilize the transition state in the same way.

IRC calculations show that methyl migration in both **1a** and **1b** leads to the same five-coordinate product, $[Ir(CO)I_3(COMe)]^-$, **4**, which has a square-pyramidal structure with the acetyl ligand apical (Figure 4c). The reaction of CO with **4** can, in principle, lead to three possible isomers of $[Ir(CO)_2I_3(COMe)]^-$. The cis,mer species **3c** would arise simply by the coordination of CO to the vacant site in **4**, but this isomer has never been observed experimentally. Consistent with this, **3c** is predicted by the DFT calculations to be the least stable of the three isomers. The formation of either of the two more stable isomers **3a** or **3b** from **4** requires prior movement of an iodide ligand into the site trans to the acetyl ligand, allowing the incoming CO ligand to coordinate cis to acetyl. To aid the modeling of these processes, we viewed the reactions as CO dissociations from **3a** and **3b**. Transition states were located for CO loss from both isomers (Figure 5), and in each case, IRC calculations showed that the five-coordinate product relaxes to generate the same structure, **4**. The transition state for CO dissociation from **3b** is computed to be lower in free energy by 24 kJ mol^{-1} (or 14.5 kJ mol^{-1} by single-point CCSD(T)) than that from **3a**. Microscopic reversibility would therefore suggest that, in the reverse direction (coordination of CO to **4**), there is a kinetic preference for formation of the trans dicarbonyl isomer **3b**. This is consistent with the experimental observations that carbonylation of **1b** (generated either photochemically[6] or thermally) gives **3b** selectively.[26]

The thermodynamics of CO dissociation from **1a** were also studied using DFT. The reaction ΔG for CO loss was computed as +79 kJ mol^{-1}, and a transition state was located with a $\Delta G^{\ddagger}$ of +147.7 kJ mol^{-1} relative to **1a**. In the transition state $\mathbf{1a^{CO‡}}$ (Figure 5), the iodide ligand trans to methyl has already started to move to the position being vacated by a CO ligand, illustrated by the widening of an I−Ir−I bond angle from 93° in **1a** to 117° in $\mathbf{1a^{CO‡}}$. Thus, a loss of CO and movement of the iodide ligand appear to be concerted, leading to a product monocarbonyl with the vacant site trans to methyl (i.e., structure **2b** from Scheme 2). It is notable that the $\Delta G^{\ddagger}$ computed by DFT for CO loss from **1a** is higher (by 27 kJ mol^{-1}) than that for methyl migration in the same complex. Thus, on the basis of the DFT results, it might be expected that thermal carbonylation of **1a** will occur via direct methyl migration rather than the CO loss mechanism via **2b**.[27] However, it should be remembered that the iodide-loss route (Scheme 1) will be competitive, especially in polar solvents which can solvate I^-.

Relation to Catalytic Carbonylation Mechanism. The potential role of **1b** during the carbonylation of **1a** merits comment. The isomerization **1a** → **1b** occurs via a CO dissociation/recombination pathway that can be induced photochemically, as shown by Volpe et al.[6] In the thermal carbonylation of **1a**, CO dissociation from **1a** could, in principle, compete with the accepted iodide dissociation route (Scheme 1) under appropriate conditions. It has been noted previously that the high-temperature carbonylation of **1a** in chlorinated solvents (PhCl or CH_2Cl_2) yields a ca. 1:1 ratio of acetyl isomers **3a** and **3b** with apparent activation parameters for the reaction of $\Delta H^{\ddagger} = 152 \pm 6$ kJ mol^{-1} and $\Delta S^{\ddagger} = 82 \pm 17$ J K^{-1} mol^{-1}.[5] In the presence of excess iodide salt, the rate is approximately halved, and the dominant product isomer is **3b**. This is consistent with a mechanism in which **3a** is formed by the iodide dissociation pathway while **3b** results from the CO-loss route. The observed activation parameters would then be a composite resulting from the two dissociative mechanisms. In the presence of a protic solvent (e.g., methanol), the carbonylation of **1a** can be achieved at much lower temperatures.[3,5] The protic solvent is considered to promote iodide dissociation, and **3a** is the dominant product isomer, suggesting that the CO-loss pathway does not compete under these conditions.

For the iridium-catalyzed methanol carbonylation process, it has been estimated that the iodide dissociation pathway accounts for ≥95% of the catalytic rate.[5] A minor alternative

(25) For the (unobserved) *trans,mer*-$[Ir(CO)_2I_3Me]^-$, the calculated $\Delta G^{\ddagger}$ for methyl migration is 123.55 kJ mol^{-1} and leads to a high-energy isomer of $[Ir(CO)I_3(COMe)]^-$ (+114.66 kJ mol^{-1} w.r.t. **4**) in which the acetyl ligand displays an agostic C−H−Ir interaction with the vacant cis coordination site.

(26) Similarly, the rhodium acetyl complex $[\{Rh(CO)I_3(COMe)_2\}^{2-}$ reacts with CO to give *trans,mer*-$[Rh(CO)_2I_3(COMe)]^-$ selectively.

(27) The single-point CCSD(T) calculations suggest $\mathbf{1a^{CO‡}}$ to be *lower* in energy than $\mathbf{1a^{MIG‡}}$ by ca. 35 kJ mol^{-1}, suggesting that CO loss might be competitive with methyl migration in **1a**. These values do not include entropic effects, which are likely significant for a dissociative process.

pathway was suggested to arise from methyl migration in **1a**, but on the basis of the present results, it can be speculated that isomerization to **1b** (via CO loss) might be responsible for a small proportion of catalytic turnover. It is unlikely, however, that **1b** would accumulate to a detectable concentration under catalytic conditions, due to its high reactivity.

Conclusion

In summary, the cis,mer isomer of $[Ir(CO)_2I_3Me]^-$ has been characterized by IR and NMR spectroscopy. This complex is carbonylated under mild conditions, in dramatic contrast to the cis,fac isomer, established as the catalyst resting state during methanol carbonylation. The difference in reactivity is attributed to the placement of a CO ligand trans to methyl, where it can stabilize the transition state for methyl migration due to its π-acceptor properties. The formation of *cis*,*mer*-$[Ir(CO)_2I_3Me]^-$ from a monocarbonyl precursor provides confirmation of the recently proposed CO-loss mechanism for photochemical carbonylation of *fac*,*cis*-$[Ir(CO)_2I_3Me]^-$.[6] Intriguingly, and counterintuitively, a CO *dissociation* mechanism may exist as a minor pathway in the iridium-catalyzed methanol carbonylation reaction.

Experimental Section

General. Solvents were purified by distillation or using a column purification system.[28] Other reagents were used as supplied: methyl iodide, ^{13}C-methyl iodide, Ph_4AsCl, (Aldrich), iridium chloride hydrate (PMO Pty Ltd.), carbon monoxide (BOC CP grade), and ^{13}C-enriched carbon monoxide (Euriso-top). Standard Schlenk techniques and glassware were used for preparative reactions.[29]

Instrumentation. Solution IR spectra were recorded on a Perkin-Elmer GX FTIR spectrometer controlled by Spectrum software using a liquid cell with CaF_2 windows (path length 0.5 mm). Stopped-flow kinetic measurements were carried out using a Hi-Tech FMA-10 rapid mixing accessory (cell path length, 1 mm) and Nicolet Magna 560 FTIR spectrometer equipped with an MCT detector. Data collection was controlled using the OMNIC Series software. ^{1}H and ^{13}C NMR spectra were recorded using Bruker AC250, AMX2-400, or DRX-500 instruments in pulse Fourier transform mode using the solvent as an internal reference. Mass spectrometry was performed on a Waters LCT time-of-flight instrument operating in either negative ion electrospray or negative ion FAB mode. Elemental analyses were determined by the University of Sheffield microanalysis service using a Perkin-Elmer 2400 instrument for CHN analysis and Schöninger flask combustion for halide determination.

Synthetic Procedures. The iridium compounds $[Ir(CO)_2I_2]AsPh_4$ and $[Ir(CO)_2I_3Me]AsPh_4$ (and their ^{13}C-labeled analogues) were synthesized using published methods.[5,10]

$[\{Ir(CO)I_3Me\}_2]\cdot 2AsPh_4$. $[Ir(CO)_2I_3Me]AsPh_4$ (0.53 g, 0.516 mmol) was dissolved in chlorobenzene (20 mL), to which MeI (2 mL) was added. After gentle reflux under N_2 at 150 °C for 5 days, an orange solid had precipitated. Upon cooling to room temperature and removal of the liquid phase by pipet, the orange precipitate was washed with diethyl ether before being dried overnight in vacuo at 100 °C. Yield: 0.43 g (84%). Anal. calcd for ($C_{26}H_{23}AsI_3IrO$): C, 31.25; H, 2.32; I, 38.10. Found: C, 31.27; H, 2.01; I, 38.21. MS (negative ion ES): *m*/*z* 617 ($[Ir(CO)I_3Me]^-$). IR: (CH_2Cl_2) ν(CO)/cm^{-1}: 2029. ^{1}H NMR ($CDCl_3$): δ 2.75 (s, 3H, C*H*$_3$), 7.6−7.9 (m, 20H, Ph_4As). Isotopicaly labeled samples were prepared from $[Ir(^{13}CO)_2I_3Me]AsPh_4$ or $[Ir(^{13}CO)_2I_3(^{13}CH_3)]AsPh_4$. For the ^{13}CO labeled compounds, $\nu(^{13}CO)$ was observed at 1981 cm^{-1} (CH_2Cl_2) with a minor $\nu(^{13}CO)$ band at 2029 cm^{-1} (estimated 80−85% ^{13}CO enrichment). For the $^{13}CH_3$ labeled analogue, resonances for the methyl group were observed at δ ^{1}H 2.75 (d, $^1J_{CH}$ 138 Hz) and δ ^{13}C −14.3. Crystals suitable for X-ray diffraction were grown by the slow diffusion of diethyl ether into a CH_2Cl_2 solution of the product.

Table 3. Crystallographic Data for $[\mathbf{2d}]\cdot 2AsPh_4$

empirical formula	$C_{26}H_{23}AsI_3IrO$
fw	999.26
space group	$P\bar{1}$
A	10.316(3) Å
B	12.214(4) Å
C	12.463(4) Å
α	72.067(5)°
β	85.988(5)°
γ	69.330(5)°
V	1396.5(8) Å^3
Z	2
T	150(2) K
λ	0.71073 Å
d_{calcd}	2.376 g cm^{-3}
μ (Mo Kα)	9.288 mm^{-1}
R1 (wR2)	0.0473 (0.1258)
Goodness-of-fit on F^2	1.075

Kinetic Measurements. The reaction of $[\{Ir(CO)I_3Me\}_2]^{2-}$ with CO was monitored using stopped-flow IR spectroscopy. The two reservoir syringes of the stopped flow unit were filled with CH_2Cl_2 solutions of $[\{Ir(CO)I_3Me\}_2]\cdot 2AsPh_4$ (1.5 mM) and CO. The solution of CO was generated either (i) by bubbling the gas through CH_2Cl_2 to ensure saturation or (ii) by stirring CH_2Cl_2 under a pressure of 8 bar CO in a Fisher Porter vessel. The second method resulted in a higher concentration of dissolved CO, although some degassing occurred between releasing the pressure and filling the reservoir syringe. However, the kinetic data obtained using either method to prepare the CO solution were comparable, indicating that, under the conditions used, the reaction rate is not sensitive to [CO]. Absorbance versus time data were extracted for the ν(CO) bands of interest and analyzed using Kaleidagraph software. Observed first-order rate constants, k_{obs}, were obtained from exponential fits to the decay of the low-frequency ν(CO) band of **2b** at 2041 cm^{-1}.

X-Ray Crystallography. Data were collected on a Bruker Smart CCD area detector with an Oxford Cryosystems low-temperature system using Mo Kα radiation ($\bar{\lambda}$= 0.71073 Å). The structures were solved by direct methods and refined by full-matrix least-squares methods on F^2. Hydrogen atoms were placed geometrically and refined using a riding model (including torsional freedom for methyl groups). Complex scattering factors were taken from the SHELXTL program package[30] as implemented on a Pentium computer. A summary of the crystallographic data is given in Table 3. Full listings of crystallographic data are given in the Supporting Information.

Computational Methods. Density functional theory calculations were performed using the SMP version of the Gaussian 03 program

(28) Pangborn, A. B.; Giardello, M. A.; Grubbs, R. H.; Rosen, R. K.; Timmers, F. J. *Organometallics* **1996**, *15*, 1518.
(29) Shriver, D. F. *The Manipulation of Air Sensitive Compounds*; McGraw-Hill: New York, 1986.
(30) Sheldrick, G. M. *SHELXTL*, revision 5.1; Bruker AXS Ltd.: Madison, WI.

package[31] with the B3LYP functional method.[32] Single-point counterpoise-corrected CCSD(T) calculations on the B3LYP optimized structures were performed using the same program package. Gaussian was compiled using the Intel ifc compiler, version 7.1, with ATLAS, version 3.6.0,[33] and the GOTO implementation of BLAS.[34] Calculations used the Stuttgart/Dresden pseudopotential on iridium and iodine[35] and the D95V basis set on all other atoms.[36] Complex geometries were optimized using high-accuracy integrals and tight optimization convergence. All energies, vibrational frequencies, and complex geometries were counterpoise-corrected using the method of Boys and Bernadi.[37] Vibrational frequencies were calculated in the harmonic approximation.

Acknowledgment. We thank BP Chemicals and EPSRC for supporting this research and Dr. Glenn Sunley for valuable discussions. We also thank Stephen Hetherington (BP Chemicals) for providing the photograph used in the cover artwork and Barry Evans for assistance with the graphical layout.

Supporting Information Available: X-ray crystallographic data, calculated ν(CO) frequencies, and DFT-optimized structures and energies (cif and pdf). This material is available free of charge via the Internet at http://pubs.acs.org.

IC8017858

(31) Frisch, M. J.; Trucks, G. W.; Schlegel, H. B.; Scuseria, G. E.; Robb, M. A.; Cheeseman, J. R.; Montgomery, J. A., Jr.; Vreven, T.; Kudin, K. N.; Burant, J. C.; Millam, J. M.; Iyengar, S. S.; Tomasi, J.; Barone, V.; Mennucci, B.; Cossi, M.; Scalmani, G.; Rega, N.; Petersson, G. A.; Nakatsuji, H.; Hada, M.; Ehara, M.; Toyota, K.; Fukuda, R.; Hasegawa, J.; Ishida, M.; Nakajima, T.; Honda, Y.; Kitao, O.; Nakai, H.; Klene, M.; Li, X.; Knox, J. E.; Hratchian, H. P.; Cross, J. B.; Bakken, V.; Adamo, C.; Jaramillo, J.; Gomperts, R.; Stratmann, R. E.; Yazyev, O.; Austin, A. J.; Cammi, R.; Pomelli, C.; Ochterski, J. W.; Ayala, P. Y.; Morokuma, K.; Voth, G. A.; Salvador, P.; Dannenberg, J. J.; Zakrzewski, V. G.; Dapprich, S.; Daniels, A. D.; Strain, M. C.; Farkas, O.; Malick, D. K.; Rabuck, A. D.; Raghavachari, K.; Foresman, J. B.; Ortiz, J. V.; Cui, Q.; Baboul, A. G.; Clifford, S.; Cioslowski, J.; Stefanov, B. B.; Liu, G.; Liashenko, A.; Piskorz, P.; Komaromi, I.; Martin, R. L.; Fox, D. J.; Keith, T.; Al-Laham, M. A.; Peng, C. Y.; Nanayakkara, A.; Challacombe, M.; Gill, P. M. W.; Johnson, B.; Chen, W.; Wong, M. W.; Gonzalez, C.; Pople, J. A. *Gaussian 03*, revision B.05; Gaussian, Inc.: Wallingford, CT, 2004.
(32) Becke, A. D. *J. Chem. Phys.* **1993**, *98*, 5648.
(33) Whaley, R. C.; Petitet, A.; Dongarra, J. J. *Parallel Computing* **2001**, *27*, 3.
(34) See http://www.cs.utexas.edu/users/flame/goto (accessed Nov. 2008).
(35) Nicklass, A.; Dolg, M.; Stoll, H.; Preuss, H. *J. Chem. Phys.* **1995**, *115*, 7348, and references therein.
(36) Dunning, T. H., Jr.; Hay, P. J. In *Modern Theoretical Chemistry*; Schaefer, H. F., III, Ed.; Plenum: New York, 1976; Vol. 3, p 1.
(37) Boys, S. F.; Bernardi, F. *Mol. Phys.* **1970**, *19*, 558.